Geophysical Prospecting EAGE EUROPEAN ASSOCIATION OF GEOSCIENTISTS & ENGINEERS

Geophysical Prospecting, 2013, **61**, 955–972 doi: 10.1111/1365-2478.12045

Flexural waves in drill-string tubulars with variable loads

Flavio Poletto*, José M. Carcione* and Giorgia Pinna

OGS (Istituto Nazionale di Oceanografia e di Geofisica Sperimentale), Borgo Grotta Gigante 42c, 34010, Sgonico, Trieste, Italy

Received March 2012, revision accepted January 2013

ABSTRACT

We revisit the equations governing the bending motions in thin rods and analyse the filtration of flexural waves in vertical drill strings pre-stressed by gravity. The aim is to study transverse drill-string vibrations at seismic frequencies for acoustic communication purposes and provide an algorithm for processing reflected and transmitted bending motions generated by downhole lateral vibrations. We obtain the dispersion equation, including attenuation due to a gravity pre-stress gradient and frequency-dependent reflection and transmission coefficients at the interface between subsequent tube intervals. We then develop a propagation-matrix algorithm to simulate flexural waves in a drill string consisting in an assembly of multiple tube sections of different dimensions. The deflection vibrations are obtained at any arbitrary recording point in the drill string. The modelling is cross-checked with a full-wave grid algorithm. The analysis shows that the waves produced by a concentrated force are partitioned in standing and propagating modes, which are calculated by using the flexural impedance of the drill string. Moreover, the reflection coefficients weakly depend on the pre-stress conditions and pre-stress has important effects for far-field signal transmission with variable weight on bit (WOB). We discuss the approximations and limits of the method with respect to realistic drilling conditions.

Key words: Pre-stress, Flexural waves, Drill string.

INTRODUCTION

Flexural waves in drill strings are easily generated during normal drilling conditions. They develop as highly dispersive modes governed by the bending properties of the drill pipes. These vibrations have important effects in the drilling process. They may be responsible for drill-string resonance and severe functioning conditions (Chin 1994). The study of flexural vibrations is also important in seismic acquisition with Vibroseis sources to eliminate the phase lag due to the baseplate flexure in acceleration measurements (Lebedev and Beresnev 2005).

Downhole drill-string bending motions are generated by bit whirling and stick slip (Vandiver, Nicholson and Shyu 1990) and it is reported that large lateral vibrations may cause twist offs and premature drill-string failure for fatigue at critical rotary speeds (Mitchel and Allen 1985; Chin 1994). These phenomena are investigated for drilling diagnostics purposes (Wolf, Zacksenhouse and Arian 1985; MacPherson, Mason and Kingman 1993; Zannoni *et al.* 1993) and numerical modelling is used to improve bending vibration analysis and predict the behaviour of drill strings (Mitchel and Allen 1985; Vandiver *et al.* 1990; Chin 1994). Monitoring downhole lateral vibrations by using surface drill-string vibration measurements is generally difficult, because flexural waves generated downhole are not easily observable at the surface (Chin 1988, 1994). Here, we discuss the propagation and attenuation of downhole flexural waves and do not obtain the results of Chin (1988, 1994) regarding trapping effects beyond a "focus located close to the neutral point, defined as the transition point between positive and negative axial stress" (see Chin 1994, p. 210). These effects or confinement of energy are negligible at the frequencies used in our simulations.

Downhole and surface measurements of drill-string vibrations are performed for seismic-while-drilling (SWD)

*E-mails: fpoletto@inogs.it, jcarcione@inogs.it

purposes, to obtain information about the drilled formations (Poletto and Miranda 2004). In common practice, this information is obtained by axial modes, which in some cases require downhole measurements to be better estimated. The borehole signals may be significantly affected by events due to bending moments and lateral vibrations of drill pipes, which are governed by the flexural behaviour of the drill string. This behaviour is revisited to determine wave propagation and resonances in the drill pipes. Knowledge of the flexural behaviour of the drill string at seismic frequencies is essential for SWD purposes. In order to assess the dynamic structural behaviour, we develop the analysis of the reflection properties of flexural waves in the drill string assumed as a layered model.

The analysis of the dispersive flexural vibrations obtained under realistic drilling conditions is a rather complex task, because different interactions and vibration phenomena occur simultaneously (Vandiver *et al.* 1990). We study the flexural motions in a vertical drill string composed of homogeneous tubulars of different dimensions. We assume a vertical drill string and neglect the conversion modes between flexural and axial waves (Kolsky 1953; Graff 1975; Shyu 1989), which may be important in curved drill strings (Drummheller 1993; Lee, Mace and Brennan 2007). We neglect the effects of drill-string rotation on bending vibrations (Mitchel and Allen 1985; Shyu 1989), which is a good approximation for the vibration signals modelled in the seismic bandwidth, the interaction with the drilling mud (free-air approximation), as well as the contacts of the drill string with the borehole wall, by assuming a vertical well, where the wall contacts are typically less important than in deviated wells. Also, other borehole modes are not considered in this work (Sinha and Asvadurov 2004). In this approximation, we neglect mud-buoyancy, which can easily be introduced into the gravity model and mud viscous damping effects. Interactions with mud and wall friction effects typically result in large energy dissipation and rapid attenuation for downhole bending vibrations in drill strings operating under realistic drilling conditions (Shyu 1989). These damping effects are not considered for the purposes of our analysis, which aims to isolate the effect of gravity rather than provide a fully realistic model of drill-string vibrations. Moreover, the filtration effects from periodic structures of drill strings with tool joints (Barnes and Kirkwood 1972; Carcione and Poletto 2000) are not considered in the examples, although they could be modelled by the algorithm. The periodicity caused by the presence of short and massive tool joints generates passband and stopband filtration effects (Poletto and Miranda 2004). Stopband effects for flexural and coupled waves in drill pipes with tool joints have been simulated by Carcione and Poletto (2000).

We use the thin-rod approximation, also known as the Euler-Bernoulli approximation, which holds when wavelengths are much larger than the radial dimensions of the pipe. The basic equations of motion of flexural waves in thin rods are given, for instance, in Kolsky (1953) and Graff (1975). We obtain the dispersion equations giving the propagating (far-field) and the standing resonant (near-field) modes in drill-string tubulars of different sizes. In this analysis, we include static tensile axial forces (pre-stress) and calculate the time-harmonic solutions of the dispersion equation at the neutral point (Bourgoyne *et al.* 1991; Chin 1994; Poletto and Miranda 2004). We compare the synthetic results obtained with and without axial pre-stress and compute the waves generated by a transverse force. The forced vibrations modes are determined by using the concept of flexural impedance (Mace 1984, 1992).

The analysis of the interaction between incident flexural waves and structural discontinuities requires the determination of the coupling, reflection and transmission effects. The approach without pre-stress loads is substantially similar to that used by Mace (1984, 1992) to study wave reflection and transmission in beams. A similar approach is used to study the transmission of flexural waves through angled structural joints of beams (Sablik 1982; Guo 1995). The structural properties of the drill string and the pre-stress conditions determine the reflection and transmission coefficients at the interfaces between different tubulars, where we equate the wavefields obtained by summing the propagating and standing modes. We calculate the reflection and transmission coefficients for propagating and standing waves in drill strings of realistic dimensions and for special boundary conditions and show that the reflection coefficients are independent of the frequency in axially unstressed (unloaded) pipes and frequency dependent in pre-stressed pipes. On the basis of the calculated reflection coefficients and complex velocities, we design a propagation-matrix algorithm to simulate flexural waves in a structural drill string including attenuation, in the far-field approximation. The attenuation results from dispersion due to the geometrical nature of the drill string with pre-loading, since we do not include a damping parameter in the model. The near-field effects at a given interface are derived from the analysis of the arrival of waves obtained by using the propagation-matrix method. Using this approach, we simulate the transmitted and reflected wavefields in a realistic drill string composed of bottom-hole assembly (BHA) and drill pipes pre-stressed by gravity. The method is tested by comparison with simulations

performed with the direct method of Carcione and Poletto (2000).

The novelty of the present technique resides on the introduction of gravity loads and a detailed reinterpretation of the physics, including the reflection and transmission effects for communication in drill strings of realistic geometry. In particular, we show how gravity pre-stress affects the wavefields obtained with different weight on bit, working both in tension and in compression.

THEORY OF FLEXURAL WAVES

Let us assume a drill pipe in a vacuum. This condition models a drill pipe in an empty borehole without wall contacts. The aim is to study the effects of the drill-string geometry and loading on wave propagation, neglecting dissipation by damping, which might reduce the communication distance. Let z be the axial coordinates and let w be the component of the lateral displacement (deflection) (Fig. 1). We assume the low-frequency approximation, which holds when the signal wavelengths are much longer than the pipe radial dimensions, i.e, we adopt the thin-rod approximation.

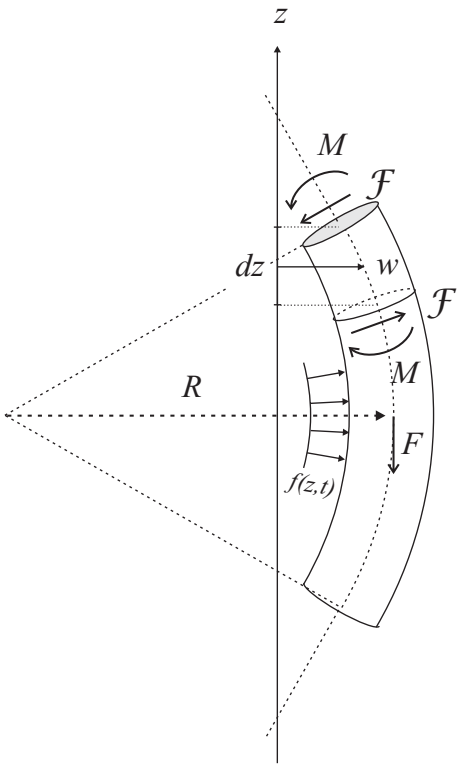

Figure 1 Pipe bending with deflection w in the (x, z)-plane. The pipe element of length dz is subject to moment M and shear force $\mathcal{F}$, while f is an external force and F is an axial tensile force.

Forces acting on the pipe

Constitutive equation

Let us consider a pipe element undergoing transverse motion, subject to a couple moment M and shear force $\mathcal{F}$ (Fig. 1). The bending moment can be expressed as $M = -YIR^{-1}$ (Love 1952), where R is the (dimensionless) radius of curvature and YI is the pipe stiffness, with Y and I the Young modulus and transverse moment of inertia. In a uniform pipe of inner and outer radii r_i and r_o, respectively, $I = \frac{\pi}{4}(r_o^4 - r_i^4)$. Using the assumption that R is large with respect to the deflection, which holds for $\partial_z w \ll 1$, we have $R = (\partial_{zz}^2 w)^{-1}$ and the bending moment can be written as

$$M = -YI\partial_{zz}^2 w. \tag{1}$$

If we neglect the rotational-inertia effect (Shyu 1989), the shear force can be expressed as $\mathcal{F} = -\partial_z M$ (Graff 1975), hence,

$$\mathcal{F} = \partial_z \left(YI\partial_{zz}^2 w\right). \tag{2}$$

Force exerted by gravity

Assume that the pipe is axially pre-stressed by a gravity tensile static force F, which is generated by the part of the pipe hanging below the investigation point (Fig. 2). We assume that axial inertia effects are negligible. The axial gravity force in an uniform pipe of cross-section A is $F = \rho Agh$, where ρ is the density of the pipe, g is the gravity constant and $h = z - z_{\mathrm{NP}}$ is the height of the hanging pipe interval between the investigation point and $z = z_{\mathrm{NP}}$, where the zero-tension point, the neutral point, is located (Bourgoyne *et al.* 1991; Chin 1994; Poletto and Miranda 2004). For convenience, we set $F/(YI) = 2b$ and $c = A\rho g/(YI)$, which gives

$$b = \frac{ch}{2}. \tag{3}$$

In the case of compression, i.e., a negative tensile force for $z < z_{\mathrm{NP}}$, b is negative. We assume that the transverse force due to gravity is proportional to the variation in the slope of the pipe deflection

$$F_g = -F\partial_z w \tag{4}$$

(Carcione and Poletto 2000).

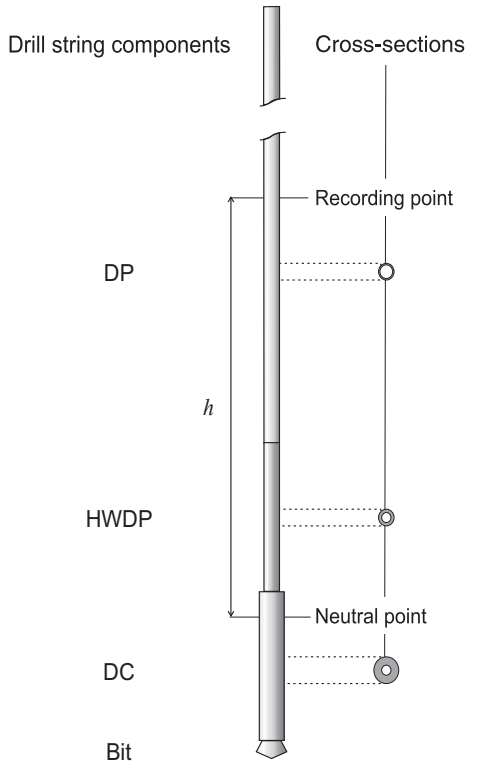

Figure 2 Main drill-string components: drill collars (DC), heavy weight drill pipes (HWDP) and drill pipes (DP), which have different cross-sections. The weight of the drill-string interval of height h above the neutral point (point where $F = 0$) causes the tensile axial force at the recording point.

Equation of motion

Flexural bending waves in thin rods undergoing transverse motion are governed by the following equation of motion

$$\rho A \partial_{tt}^2 w = -\partial_z(\mathcal{F} + F_g) + f \tag{5}$$

(Kolsky 1953; Graff 1975, Carcione and Poletto 2000), where f is an external, distributed lateral force (Fig. 1). Substituting equations (2) and (4) into equation (5) yields

$$\rho A \partial_{tt}^2 w + \partial_{zz}^2 \left(YI \partial_{zz}^2 w\right) - \partial_z(F \partial_z w) - f = 0, \tag{6}$$

or

$$a^2 \partial_{tt}^2 w + \partial_{zzzz}^4 w - c\partial_z w - 2b\partial_{zz}^2 w = 0, \tag{7}$$

where we have assumed a uniform pipe, $f = 0$, used equation (3) and defined

$$a = \sqrt{\frac{\rho A}{YI}}. \tag{8}$$

Equation (6) is used to model flexural waves in drill strings of realistic geometry with variable properties, while equation (7) allows us to study the physics analytically.

Plane-wave analysis

A plane-wave solution is given by $w(t, z) = \exp[\mathrm{i}(\omega t - kz)]$, where ω is the angular frequency, k is the wavenumber and $\mathrm{i} = \sqrt{-1}$. Substituting this equation into equation (7), we obtain the dispersion equation (Chin 1988)

$$k^4 + 2b\,k^2 + \mathrm{i}ck - a^2\omega^2 = 0. \tag{9}$$

Equation (9) has four solutions (see the Appendix) and due to the term ick, all the solutions are complex. The phase velocity and attenuation factor are given by

$$v_p = \left[\mathrm{Re}\left(\frac{1}{v}\right)\right]^{-1} \quad \text{and} \quad \alpha = -\mathrm{Im}\left(\frac{\omega}{v}\right), \tag{10}$$

where $v = \omega/k$ is the complex velocity, while the group velocity is $v_g = \partial_\kappa \omega$. Even if we can assume that in vertical wells damping due to borehole wall contact is weak (Chin 1994), additional damping can easily be included to model viscous dissipation effects in non-rotating pipes (see Dunayewsky, Abbassian and Judzis 1993; Chin 1994, p. 223; Connaire *et al.* 2008). In the following, we model non-viscous attenuation.

Absence of gravity effects

In the absence of gravity effects ($b = c = 0$), the roots are

$$k_1 = k_0, \quad k_2 = -k_0, \quad k_3 = \mathrm{i}k_0, \quad k_4 = -\mathrm{i}k_0, \quad k_0 = \sqrt{a\omega}. \tag{11}$$

The first two roots correspond to progressive and regressive waves (far-field modes), while k_3 and k_4 are static (or standing) modes. One root is an unstable diverging mode and the other corresponds to standing energy stored in stable local resonances, i.e., near-field effects (White 1965; Graff 1975; Carcione and Poletto 2000). The standing stable waves vanish at distances for which $|k_0 z| \gg 1$. The standing modes are localized in the near-field region defined by the condition $|z| \leq 1/k_0$. The phase velocity of the propagating modes is $v_p = \pm(\omega/k_0) = \pm\sqrt{\omega/a}$ when there is no attenuation and the group velocity is $v_g = 2v_p$. The general harmonic solution including near-and far-field terms has the form

$$\begin{aligned} w(t, z) = \exp(\mathrm{i}\omega t)[&B_1 \exp(-\mathrm{i}k_0 z) + B_2 \exp(\mathrm{i}k_0 z) \\ &+ B_3 \exp(-k_0 z) + B_4 \exp(k_0 z)] \end{aligned} \tag{12}$$

(Lindsay 1934; Graff 1975), where B_1, B_2, B_3, B_4 are constant coefficients of progressive waves, regressive waves, local stored (resonant) energy and an unbounded response for increasing $z > 0$, respectively.

Gravity effects with a weak gradient

In several practical cases, as in pipe elements far from the neutral point (see next section), the gradient of the tensile force is negligible with respect to the tensile force itself, i.e., $\partial_z F \ll F$ and $c \cong 0$. When the pipe stiffness YI is negligible, we obtain the well-known non-dispersive equation for transverse vibrations in a string under tension (Graff 1975). Assume positive tension, i.e., $b > 0$. Equation (9) has two real solutions

$$k_{1,2} = \pm\sqrt{-b + \sqrt{b^2 + a^2\omega^2}}, \tag{13}$$

which correspond to propagating modes without attenuation and two imaginary solutions, given by

$$k_{3,4} = \pm \mathrm{i}\sqrt{b + \sqrt{b^2 + a^2\omega^2}}. \tag{14}$$

Similar real and imaginary roots are obtained if we assume negative tension, i.e., compression, i.e., $b < 0$. Note that in compression and for real values of the frequency ω, the real positive root assumes the lower limit $\sqrt{2|b|} = \sqrt{|F|/YI}$, representing the wavenumber in an axially-loaded pipe section under a critical-buckling condition. The group velocity of the flexural wave in a pre-stressed pipe with a negligible pre-stress gradient is

$$v_g = \frac{2\sqrt{(b^2 + a^2\omega^2)(-b + \sqrt{b^2 + a^2\omega^2})}}{a^2\omega} \tag{15}$$

(Chin 1988). The group velocity $v_g(b)$ has the minimum $v_g(b_{min}) = 3^{-3/4}\ 2v_g(0) \cong 0.88\ v_g(0)$, where $b_{min} = a\omega/\sqrt{3}$. We obtain that the minimum group velocity in a pipe under tension is about 88% of that in an unstressed pipe.

Neutral point

A particular case in which the previous approximation of having a negligible gradient of the tensile force with respect to the tensile force itself is not valid, is when the axial loads pass from tension to compression. This occurs at the neutral point z_{NP} and the tension F vanishes in equation (7). It is equivalent to consider $b = 0$. The solutions of the dispersion equation are given in the Appendix [equation (A4)]. All the solutions are complex, so that there are attenuation effects in the propagation through the neutral point.

MODES IN A UNIFORM PIPE

We now analyse the vibrations generated in a pipe by a point source applied at $z = 0$, namely

$$s(t, z) = \exp(\mathrm{i}\omega t)\delta(z). \tag{16}$$

We study the solutions in a uniform, unstressed and unbounded pipe [equation (6) with $F = 0$]. Let w_d and w_u be the harmonic solutions for $z < 0$ and $z > 0$, respectively. These solutions include the regressive and progressive waves (far-field terms) of amplitudes A_d and A_u and the stable standing modes (near-field terms) of amplitudes B_d and B_u, respectively. We have

$$\begin{aligned} w_d(t, z) &= A_d \exp[\mathrm{i}(\omega t + kz)] + B_d \exp(\mathrm{i}\omega t + kz), \\ w_u(t, z) &= A_u \exp[\mathrm{i}(\omega t - kz)] + B_u \exp(\mathrm{i}\omega t - kz), \end{aligned} \tag{17}$$

where we have neglected the unstable diverging terms. Because of the symmetry of the problem and because of the continuity of the solutions $w_d(t, 0) = w_u(t, 0)$ at the source location, we can reduce the number of constants, thus obtaining the amplitudes of the forced waves in equation (17) as

$$\begin{aligned} A_f &\equiv A_d = A_u, \\ B_f &\equiv B_d = B_u. \end{aligned} \tag{18}$$

To solve for the unknown coefficients A_f and B_f, we require continuity in the slope of the solutions at $z = 0$ (Graff 1975). The slopes are given by $\partial_z w_d$ and $\partial_z w_u$. We obtain

$$-\mathrm{i}A_f - B_f = \mathrm{i}A_f + B_f. \tag{19}$$

Another condition is obtained by integrating the equation of motion in a small interval including $z = 0$ with width tending to zero, which gives

$$\partial^3_{zzz} w_u - \partial^3_{zzz} w_d = \frac{1}{YI} \tag{20}$$

(see Graff 1975, p. 161) and

$$\mathrm{i}A_f - B_f = \frac{1}{2YIk^3}. \tag{21}$$

Solving equations (19) and (20), we obtain

$$A_f = \mathrm{i}B_f \quad \text{and} \quad B_f = -\frac{1}{4YIk^3}. \tag{22}$$

Substituting these expressions into equation (17) yields

$$\begin{aligned} w_d(t, z) &= B_f \exp(\mathrm{i}\omega t)[i\exp(\mathrm{i}kz) + \exp(kz)], \\ w_u(t, z) &= B_f \exp(\mathrm{i}\omega t)[i\exp(-\mathrm{i}kz) + \exp(-kz)]. \end{aligned} \tag{23}$$

It follows that a point force $\delta(z)$ generates propagating and standing waves of equal amplitude in an unbounded unstressed string.

Characteristic mechanical impedance

To obtain a relationship between force and deflection, we use the concept of characteristic mechanical impedance of flexural waves, Z, which is defined as the shear force to the lateral particle-velocity ratio (Lindsay 1934; Mace 1984; Drumheller 2002). For harmonic vibrations, we have

$$Z = \frac{\mathcal{F}}{\dot{w}} = \frac{\mathcal{F}}{i\omega w} = \left(\frac{1}{\mathrm{i}\omega w}\right)\partial_z M, \tag{24}$$

where the dot above a variable denotes a time derivative.

As the excitation force generates both propagating and standing waves, the mechanical impedance is complex. This condition corresponds to the fact that, in the far-field, the force and particle velocity are in phase, so that the energy is expended in the form of waves that are radiated away in an unbounded pipe. Conversely, in the standing near-field modes, the force and particle velocity are out of phase by $\pm\pi/2$, so that the average energy expended is zero. Substituting equation (22) into equation (17) and using equations (1) and (24), we obtain the impedances

$$Z_u = -\frac{(1+\mathrm{i})IYk^3}{\omega} \quad \text{and} \quad Z_d = \frac{(1+\mathrm{i})IYk^3}{\omega}, \tag{25}$$

which, in uniform unstressed pipes, can be written as $Z_{u,d} = \mp(1+\mathrm{i})v_p\rho A$. We obtain opposite impedances because the point force generates opposite shear forces and the same deflection at both sides. Using equations (8) and (11), we can express the impedances for a uniform unstressed pipe as

$$Z_u = -(1+\mathrm{i})(A\rho)^{3/4}(IY)^{1/4}\sqrt{\omega} \quad \text{and} \quad Z_d = -Z_u. \tag{26}$$

This means that a point force with a constant amplitude spectrum generates a transverse particle velocity proportional to $1/\sqrt{\omega}$.

REFLECTION AND TRANSMISSION COEFFICIENTS

A drill string of realistic geometry is an assembly composed of tubes of different dimensions and properties (Fig. 2) (Bourgoyne *et al.* 1991; Poletto and Miranda 2004). Starting from the bit, these are the drill collars (DC), the heavy weight drill pipes (HWDP, or more simply HW in the subscripts) and the drill pipe (DP). DC and HWDP form the bottom-hole assembly (BHA). The neutral point z_{NP} is typically located in the DC section, which is more massive and can work both under tension and compression. The HWDP and DP sections work in tension.

Table 1 Dimensions of the drill string

Pipe section	d_o (in)	d_i (in)	Length (m)
DC	8	2 13/16	145
HWDP	5	3	145
DP	5	4 3/4	2500

We assume, with a reasonable approximation, that the modelled drill string is an assembly of uniform tubes (Table 1). We then use the equation for homogeneous pipes in the uniform sections and calculate explicit boundary conditions at the interfaces between different pipes. Without loss of generality, we first study the wave propagation in a pipe made of two homogeneous semi-infinite tubes of different radial dimensions. Let these tubes be denoted by T1 and T2 (Fig. 3).

When a progressive (upgoing) flexural wave of unit amplitude, propagating in T1, hits the interface between T1 and T2, a regressive (downgoing) flexural wave is reflected in T1 and a progressive flexural wave is transmitted in T2. The incident wave also generates local resonant energy, which is

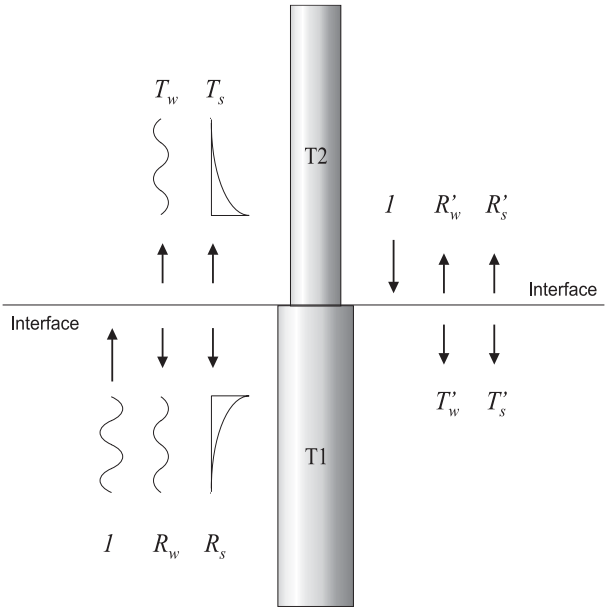

Figure 3 Reflection and transmission coefficients for axial waves in a drill string made of two semi-infinite sections. When a unit input signal hits the interface, a regressive signal R_w and a standing resonant wave R_s are generated in T1. A transmitted progressive signal T_w and a standing resonant mode T_s are generated in T2. R'_w, R'_s, T'_w and T'_s are the coefficients at the opposite side of the interface.

stored in both tubes. We assume, without loss of generality, that the interface is located at $z=0$. In T1, we have

$$w_1 = \exp[\mathrm{i}(\omega t - k_1 z)] + R_w \exp[\mathrm{i}(\omega t + k_1 z)] + R_s \exp(\mathrm{i}\omega t + k_1 z), \tag{27}$$

where k_1 is written for k_{01} [last term of equation (11)] in T1 and where R_w and R_s are reflection coefficients of the regressive wave and the standing wave resulting in local stored energy (at $z<0$), respectively. A similar relation can be written for the energy transmitted in T2,

$$w_2 = T_w \exp[\mathrm{i}(\omega t - k_2 z)] + T_s \exp(\mathrm{i}\omega t - k_2 z), \tag{28}$$

where T_w and T_s are the transmission coefficients of the progressive wave and of the standing wave resulting in local stored energy (at $z>0$), respectively.

We determine the four coefficients R_w, R_s, T_w and T_s by using the boundary conditions at the interface. Coupled equations are obtained by requiring continuity of the deflection w, the slope $\partial_z w$, the bending moment M [equation (1)] and the shear force $\mathcal{F}$ [equation (2)] (Graff 1975). At $z=0$ we have

$$\begin{aligned} w_1 &= w_2, \\ \partial_z w_1 &= \partial_z w_2, \\ M_1 &= M_2, \\ \mathcal{F}_1 &= \mathcal{F}_2. \end{aligned} \tag{29}$$

Combining equations (27), (28) and (29), we obtain

$$\begin{pmatrix} 1 \\ \mathrm{i} \\ -1 \\ -\mathrm{i} \end{pmatrix} = \begin{pmatrix} -1 & -1 & 1 & 1 \\ \mathrm{i} & 1 & i\gamma & \gamma \\ 1 & -1 & -\xi\gamma^2 & \xi\gamma^2 \\ -\mathrm{i} & 1 & -\mathrm{i}\xi\gamma^3 & \xi\gamma^3 \end{pmatrix} \begin{pmatrix} R_w \\ R_s \\ T_w \\ T_s \end{pmatrix}, \tag{30}$$

where

$$\gamma = \frac{k_2}{k_1} \quad \text{and} \quad \xi = \frac{I_2}{I_1}. \tag{31}$$

In unstressed pipes we have, according to equations (8) and (11),

$$\gamma = \left(\frac{I_1 A_2}{I_2 A_1}\right)^{\frac{1}{4}}, \tag{32}$$

where it is assumed that the density and the Young modulus are constant, while in pipes pre-stressed by the axial tensile force F we have, according to equations (3) and (13),

$$\gamma = \sqrt{\frac{\sqrt{q_2^2+s_2}-q_2}{\sqrt{q_1^2+s_1}-q_1}}, \quad q_i = \frac{F}{2YI_i}, \quad s_i = \frac{\rho\omega^2 A_i}{YI_i}. \tag{33}$$

We obtain explicit solutions for the reflection and transmission coefficients as

$$\begin{aligned} R_w &= \frac{-\mathrm{i}(1+2\mathrm{i}\gamma\xi-2\gamma^2\xi-2\mathrm{i}\gamma^3\xi+\gamma^4\xi^2)}{1+2\gamma\xi+2\gamma^2\xi+2\gamma^3\xi+\gamma^4\xi^2}, \\ R_s &= \frac{(-1+\mathrm{i})(-1+\gamma^4\xi^2)}{1+2\gamma\xi+2\gamma^2\xi+2\gamma^3\xi+\gamma^4\xi^2}, \\ T_w &= \frac{2(1+\gamma)(1+\gamma^2\xi)}{\gamma(1+2\gamma\xi+2\gamma^2\xi+2\gamma^3\xi+\gamma^4\xi^2)}, \\ T_s &= \frac{2(1+\mathrm{i}\gamma)(-1+\gamma^2\xi)}{\gamma(1+2\gamma\xi+2\gamma^2\xi+2\gamma^3\xi+\gamma^4\xi^2)}. \end{aligned} \tag{34}$$

From equations (32) and (33) it follows that these coefficients are frequency independent and frequency dependent in unstressed and pre-stressed pipes, respectively. The fact that the reflection coefficients are complex means that the presence of local resonant effects produces a change in the phase of the back-propagating reflected waves. Conversely, the transmission coefficient T_w is real, hence there is no change of phase in the transmitted wave. The phase of the evanescent-mode reflection coefficient R_s is equal to $-\pi/4$.

Coefficients at opposite sides of the interface

We apply a rule that relates the coefficients at the opposite sides of the interface. They are obtained by exchanging k_1 for k_2, hence by taking $\gamma' = \gamma^{-1}$ and $\xi' = \xi^{-1}$ for γ and ξ, respectively. This gives

$$\begin{aligned} R'_w &= \frac{-i(1-2i\gamma\xi-2\gamma^2\xi+2i\gamma^3\xi+\gamma^4\xi^2)}{1+2\gamma\xi+2\gamma^2\xi+2\gamma^3\xi+\gamma^4\xi^2}, \\ R'_s &= \frac{(1-i)(-1+\gamma^4\xi^2)}{1+2\gamma\xi+2\gamma^2\xi+2\gamma^3\xi+\gamma^4\xi^2}, \\ T'_w &= \frac{2\gamma^2\xi(1+\gamma)(1+\gamma^2\xi)}{1+2\gamma\xi+2\gamma^2\xi+2\gamma^3\xi+\gamma^4\xi^2}, \\ T'_s &= \frac{-2\gamma^2\xi(i+\gamma)(-1+\gamma^2\xi)}{1+2\gamma\xi+2\gamma^2\xi+2\gamma^3\xi+\gamma^4\xi^2}. \end{aligned} \tag{35}$$

We may relate the mechanical impedances using equation (26). From equation (31), we have

$$\zeta \equiv \frac{Z_2}{Z_1} = \gamma^3\xi. \tag{36}$$

Therefore, the relations between the set of coefficients in the unstressed case can be written as

$$R'_w = -R^*_w, \quad R'_s = -R_s, \quad T'_w = \zeta T_w, \quad T'_s = -\mathrm{i}\zeta T^*_s, \qquad (37)$$

where "*" denotes a complex conjugate.

Special cases of reflecting boundaries

We study two special cases of reflection of flexural waves in semi-infinite strings bounded at only one end (Graff 1975).

Fixed end

We assume the drill string fixed at its end, which is equivalent to setting the radial dimensions of T2 much larger than those of T1, the latter assumed to be a reference section with constant properties. Taking the limits $\xi \to \infty$ and $\gamma \to 0$ in equation (34), for infinite radial dimensions of T2, we have

$$R_w = -\mathrm{i}, \quad R_s = -1 + \mathrm{i}, \quad T_w = 0, \quad T_s = 0. \qquad (38)$$

Free end

We assume the drill string free at its end, which is equivalent to setting the radial dimensions of T2 negligible with respect to those of T1. Taking the limits $\xi \to 0$ and $\gamma \to \infty$ in equation (34), for zero radial dimensions of T2, we obtain

$$R_w = -\mathrm{i}, \quad R_s = 1 - \mathrm{i}, \quad T_w = 2, \quad T_s = -2\mathrm{i}. \qquad (39)$$

Equations (38) and (39) can be used to model the boundary conditions at the ends of a drill pipe.

PROPAGATION-MATRIX METHOD (FAR FIELD)

We use a classical propagation-matrix method to simulate far-field waves in a drill string of realistic geometry. We assume that the reflecting interfaces along the drill string are separated far away, in the sense that the local (near-field) standing waves generated at a given interfaces are negligible at the neighbouring interfaces. This is a realistic assumption, as far as we model a drill string made of components having lengths of the order of tens of metres, i.e., lengths $\gg 1/k_0$, with signals having frequencies of some tens of Hz or more. The layout of the one-dimensional drill-string transmission line is shown in Fig. 4, where $j = 1, \ldots, J$ is the interval index, $l_j = z_{j+1} - z_j$ is the interval length, U_j, D_j and U'_j and D'_j are the upper-side and lower-side upgoing and downgoing waves, respectively

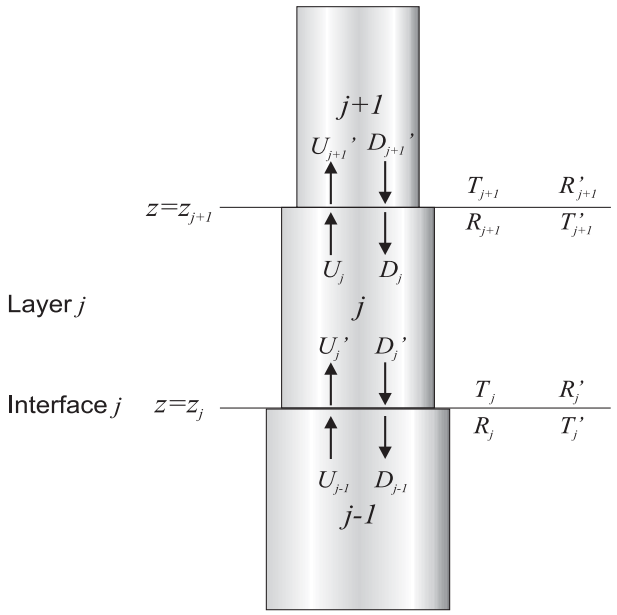

Figure 4 Layered model used for the propagation-matrix method, where j is the layer (interface) index and U_j, D_j and U'_j and D'_j are propagating upgoing and downgoing wavefields at the top and bottom of the j-th layer, respectively.

and R_j, T_j and R'_j and T'_j are the upper-side and opposite-side coefficients, respectively, of the j-th interface connecting intervals $j-1$ and j at $z = z_j$ (see Fig. 3) (we omit the subindex 'w' in the coefficients for clarity). We propagate only reflected and transmitted waves by using the coefficients R, T, R' and T' at the j-th interface. We have

$$\begin{aligned} U'_j &= T_j U_{j-1} + R'_j D'_j \\ D_{j-1} &= R_j U_{j-1} + T'_j D'_j. \end{aligned} \qquad (40)$$

From equations (40) and (37) we obtain the relation between waves at the opposite side of the j-th interface as

$$\begin{pmatrix} U'_j \\ D'_j \end{pmatrix} = \frac{1}{T'_j} \begin{pmatrix} 1 & R'_j \\ -R_j & 1 \end{pmatrix} \begin{pmatrix} U_{j-1} \\ D_{j-1} \end{pmatrix}, \qquad (41)$$

where we have used the property $T_j T'_j - R_j R'_j = 1$, expressing conservation of energy for propagating waves (Muggleton *et al.* 2007). The wavefields at the $(j+1)$-th interface are computed from those at the j-th interface by means of the propagation delays Δ_j in the j-th interval,

$$\Delta_j(\omega) = \int_{z_j}^{z_{j+1}} \frac{1}{v_p^{(j)}(\omega)} dz, \qquad (42)$$

where v_p is the phase velocity defined in equation (10). We obtain

$$\begin{pmatrix} U_j \\ D_j \end{pmatrix} = \mathbf{Q}_j \begin{pmatrix} U_{j-1} \\ D_{j-1} \end{pmatrix}, \tag{43}$$

where

$$\mathbf{Q}_j = \frac{1}{T'_j} \Lambda_j \begin{pmatrix} 1 & R'_j \\ -R_j & 1 \end{pmatrix} \tag{44}$$

and

$$\Lambda_j = \begin{pmatrix} \exp\left(-\mathrm{i}\omega\Delta_j\right) & 0 \\ 0 & \exp\left(\mathrm{i}\omega\Delta_j\right) \end{pmatrix}. \tag{45}$$

In a string made of a cascade of intervals, the propagation matrix is obtained as

$$\mathbf{Q}(\omega) = \begin{pmatrix} q_{11} & q_{12} \\ q_{21} & q_{22} \end{pmatrix} = \prod_{j=J}^{1} \mathbf{Q}_j(\omega). \tag{46}$$

With the pre-stress gradient not equal to zero, the delays Δ_j are complex and matrix $\mathbf{Q}$ includes (far-field) attenuation effects. With some modifications, by using equation (46), we can calculate the propagating wavefields in every position of the drill string. In the vicinity of the j-th interface standing waves are generated by the arrival of the upgoing U_{j-1} and downgoing D'_j waves. These near-field modes are obtained as

$$\left(D'_j R'_{sj} + U_{j-1} T_{sj}\right) \exp[-k_j(z - z_j)], \tag{47}$$

and

$$\left(D'_j T'_{sj} + U_{j-1} R_{sj}\right) \exp[k_{j-1}(z - z_j)], \tag{48}$$

in the intervals j and $j - 1$, respectively.

DRILL-STRING TIME-DOMAIN WAVEFIELDS

Without loss of generality, we calculate the upgoing U and downgoing D wavefields for the particle velocity, i.e., the time derivative $\dot{w}$ of the deflection w. In this example, the drill string is assumed open at the lower side of the DC, i.e., the bit is a free end [equation (39)], while at the upper side the drill pipes are unbounded (DP of infinite length). Let $s(\omega)$ be the source signal in the frequency domain. Note that this source corresponds to the particle-velocity wavefield obtained from the shear force $\mathcal{F}$ by impedance equation (24). This signal is injected at the lower end of the string (see the propagation model shown in Fig. 5). Let $\dot{w}_T(\omega)$ and $\dot{w}_R(\omega)$ be the particle-velocity signal transmitted at the recording point (Fig. 5) and the signal reflected at the bit, respectively. We obtain

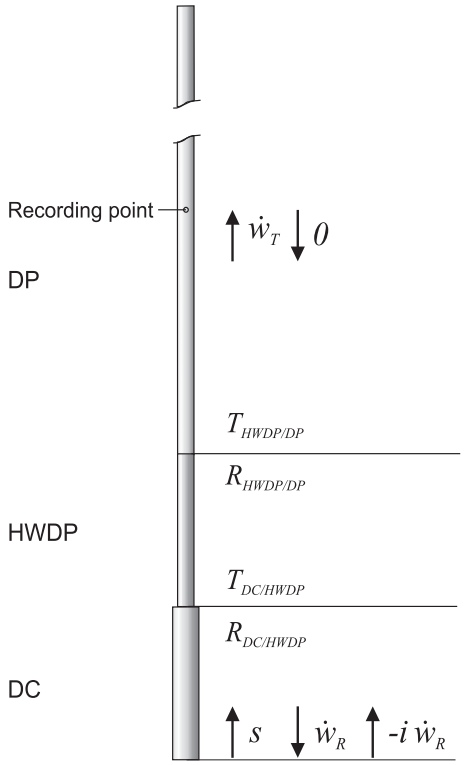

Figure 5 Reflection model of the drill string corresponding to Table 1 used for the simulation of flexural wavefields. $s(t)$ is an input signal (only propagating wave) and $\dot{w}_R(t)$ and $\dot{w}_T(t)$ are the reflection signal at the bit and the transmission signal recorded in the DP, respectively.

$$\begin{pmatrix} \dot{w}_T \\ 0 \end{pmatrix} = \mathbf{Q}_{\mathrm{HW,DP}} \Lambda_{\mathrm{DC}} \begin{pmatrix} s - \mathrm{i}\dot{w}_R \\ \dot{w}_R \end{pmatrix}, \tag{49}$$

where we used equations (38), (45) and (46) and $\mathbf{Q}_{\mathrm{HW,DP}}$ is the propagation matrix in the HWDP and DP. Using the notation q_{ij} to denote the elements of the matrix $\mathbf{Q}_{\mathrm{HW,DP}}\Lambda_{\mathrm{DC}}$, we obtain the solutions

$$\dot{w}_T = \frac{(q_{11}q_{22} - q_{12}q_{21})s}{q_{22} - \mathrm{i}q_{21}} \tag{50}$$

and

$$\dot{w}_R = -\frac{q_{21}s}{q_{22} - \mathrm{i}q_{21}}. \tag{51}$$

The time histories of the reflected and transmitted signals are obtained as inverse Fourier transforms.

EXAMPLES

The properties of the different sections of the drill string of Fig. 5 are given in Table 1. The material properties of all the components are the same (steel), i.e., $\rho = 7840$ kg/m^3 and $Y = 206$ GPa. This example corresponds, with a reasonable approximation, to a drill string used in a borehole section drilled by a drill bit with a diameter of 12 1/4 inches. In our analysis, all these elements are assumed to be uniform tubes, which differ essentially by their inner and outer diameters. In this approximation we neglect the presence in the DC section of the short-length elements (stabilizers), which act as wall-contact tools. These elements can be taken into account in the model for a more detailed analysis.

Phase velocity (10) corresponding to the DC, HWDP and DP sections together with the group velocity of the DP section are shown in Fig. 6(a), and the velocities corresponding to the DP section, with and without gravity pre-stress, are shown in Fig. 6(b). The tension is due to the weight exerted by a 2500 m DP section and by a 145 m HWDP section. In this case, we assume that the neutral point z_{NP} is located at the DC/HWDP interface, i.e., we have the limit case in which the weight on bit (WOB) equals the weight of the DC.

Figure 7 shows the phase velocity versus length of the hanging DP interval. A larger distance in the DP section corresponds to a higher tension at the recording point. The phase velocity is calculated at frequencies of 10, 20 and 40 Hz in the pre-stressed case and compared to that calculated at 10 Hz in the unstressed case. This example shows that the effect of pre-stress becomes dominant in the drill pipes at large distances from the bottom hole.

In general, the tensile force in the drill string changes with WOB. Dynamic effects due to variations in the WOB may cause fluctuations of the neutral point position (Chin 1994; Poletto and Miranda 2004) and may affect the pre-stress tensile forces and, hence, the flexural properties of the drill string (Vandiver *et al.* 1990). A plot of the tensile force versus distance (z) from the bit is shown in Fig. 8(a). In this case, the WOB is 20 ton (200 kN) and the neutral-point position (Bourgoyne *et al.* 1991; Poletto and Miranda 2004) at $z_{NP} = \mathrm{WOB}/(9.81\rho A_{DC}) \cong 90$ m is indicated by the arrow. Figure 8(b) shows the real part of the wavenumber (see equation (A1)) in the pre-stressed pipes of Fig. 8(a). The data are shown at frequencies of 50 Hz, 10 Hz and 1 Hz. We can notice the different trend of the curves calculated at different frequencies in the DC section, where the pre-stress gradient is larger, relative to the trend of the curves in the HW and DP sections. The interpretation of this result is that the gravity gradient effect becomes relatively more important at low frequencies for flexural dispersion in the DC section.

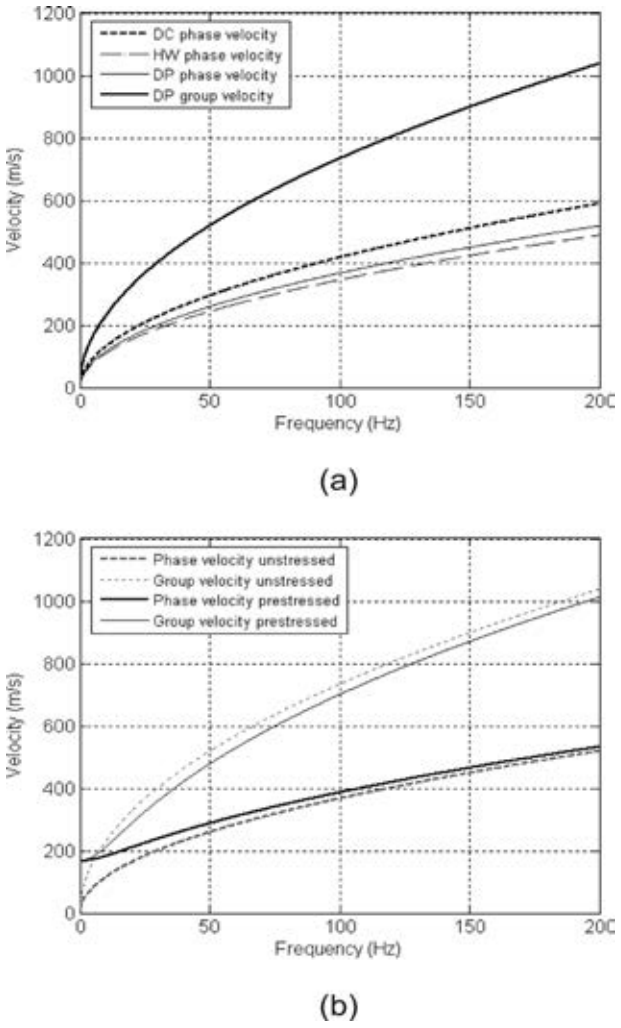

Figure 6 Dispersion curves of flexural waves in the unstressed case (a). The velocities are calculated for the drill-string sections of Table 1. Dispersion curves of the flexural waves for the 5 in the DP section of Table 1, pre-stressed by gravity, compared to the unstressed case (b). The recording point is located at 2500 m above the HWDP/DP interface (Fig. 2). The tension is assumed constant (with gradient equal to zero).

Let us analyse the attenuation of the propagating modes (far-field). Figures 9 and 10 show the amplitude attenuation coefficient $\exp(\alpha z)$ [equation (10)], versus frequency and distance, respectively. The far-field attenuation is due to the axial gradient of pre-stress that introduces an imaginary part in the solutions of the dispersion equation. At 10 Hz, the amplitude of the imaginary component of the wavenumber solutions is small, about 1% that of the real part and the attenuation is

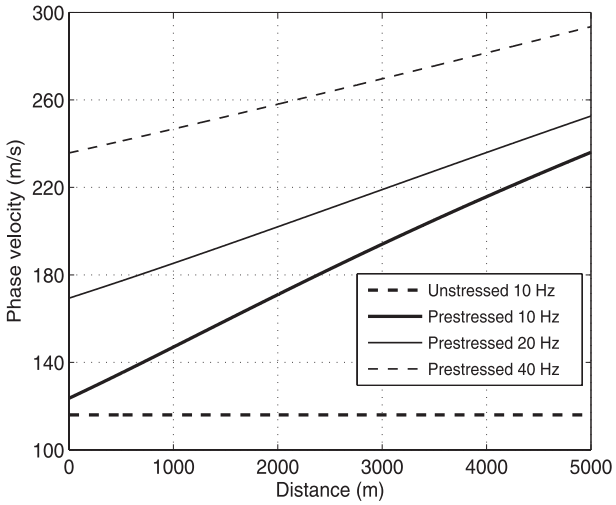

Figure 7 Phase velocity in the DP with pre-stress. The velocity is shown for different signal frequencies versus length of the DP above the HWDP, i.e., the zero distance is set at the HWDP/DP interface. In this example, the neutral point is located at this interface so that the tension due to the HWDP section weight is not nil at $z = 0$ in the DP section. For this reason, the pre-stressed and unstressed lines calculated at 10 Hz do not coincide at $z = 0$.

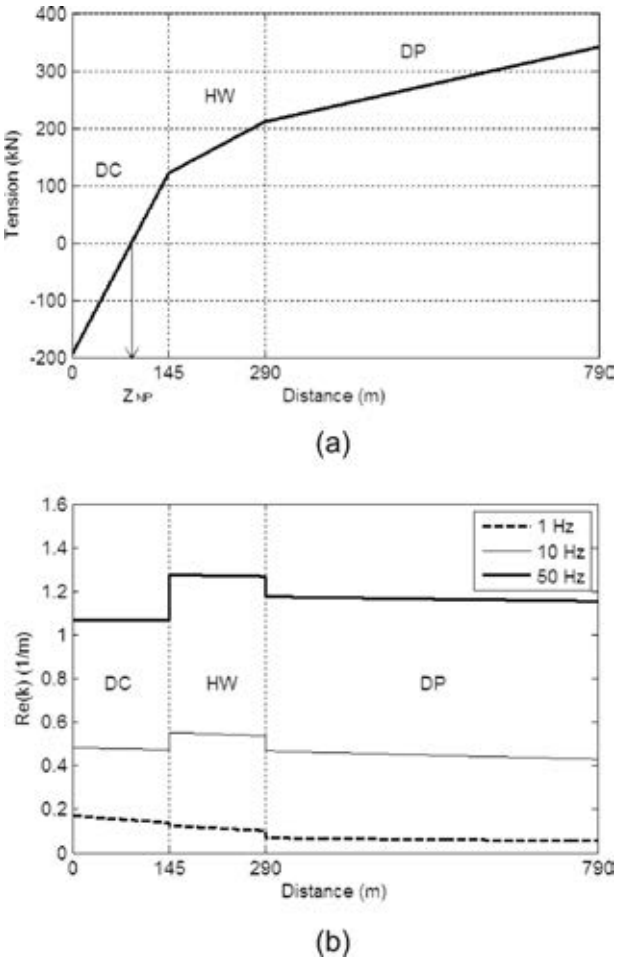

Figure 8 Tensile force in a drill string composed of DC, HWDP and DP (see Table 1) with WOB = 20 ton (a). The zero distance is set at the bit position. The arrow indicates the neutral point at z_{NP}. Below this point, the DC is in compression. Buoyancy mud forces are not included. Real part of the wavenumber in the pre-stressed drill string corresponding to Fig. 8(a) (b). We can notice the variation of the curves in the DC section, where the pre-stress gradient is larger, relative to those in the HW and DP sections.

not strong (Fig. 9). The cumulative far-field attenuation effects become more important at large distances and lower frequencies (Chin 1988, 1994). For example, at a distance of 2 km and a frequency of 1 Hz, the amplitude decay is about 0.4 (Fig. 10).

The standing resonant modes, consisting in near-field vibrations, are strongly damped with increasing axial distance. The attenuation distance beyond which the near-field effects become negligible with respect to the far-field effects, is $1/k_0$, where k_0 is given in equation (11). Figure 11 shows the near-field attenuation distances versus frequency, corresponding to the unstressed drill pipe sections indicated in Table 1. The near-field distance $1/k_0$ may be used as a reference distance to determine the limit between the near-field and far-field approximations and, for instance, to evaluate the distance for recording positions from contact tools (stabilizers), which can be modeled in bottom-hole assemblies.

The attenuation of the standing modes versus distance is shown in Fig. 12. We observe that at 10 Hz and 6 m, the amplitude of the resonant modes in the HWDP section decays by nearly 30 dB. Since we use the approximation that the typical length of the uniform drill-string parts is of the order of several tens of metres (in this case the length of the HWDP is 145 m), the resonant modes vanish at these distances (at 145 m we obtain a decay of approximately 700 dB at 10 Hz in the HWDP). The implication is that we can calculate the wave propagation using the reflection and transmission coefficients at each interface by assuming two semi-infinite tube sections.

We validate this assumption and the propagation-matrix method presented here by comparing the results with those of a full-wave direct solver (Carcione and Poletto 2000). In this algorithm, the flexural vibrations including the standing modes are computed with a 4th-order Runge-Kutta technique and the spatial derivatives are calculated with the Fourier pseudospectral method by using the Fast Fourier Transform (FFT) (Carcione 2007). These approximations are infinitely

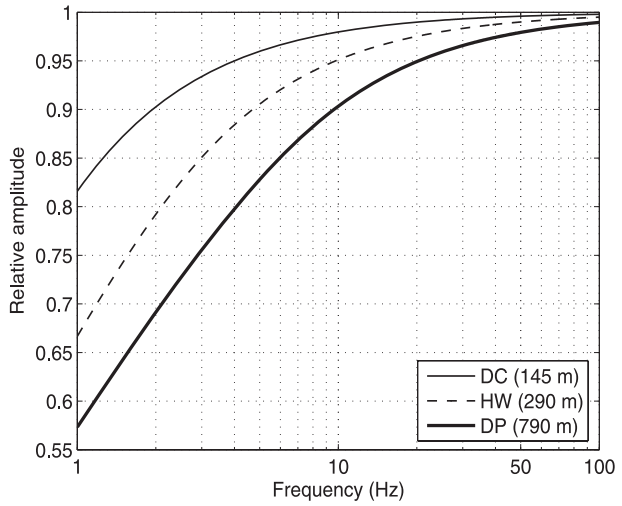

Figure 9 Attenuation of the far-field waves versus frequency for a signal of 10 Hz corresponding to the pre-stressed drill string of Fig. 8(a). The recording points are simulated at the end of the DC section ($z = 145$ m), at the end of the HWDP section ($z = 290$ m) and at 500 m in the DP section ($z = 790$ m).

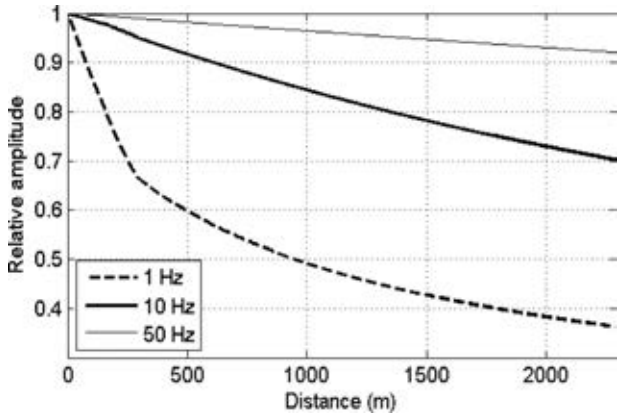

Figure 10 Attenuation of the far-field waves versus distance in a drill string with a pre-stress gradient for different frequencies (see Fig. 8a). The zero distance is set at the bit position.

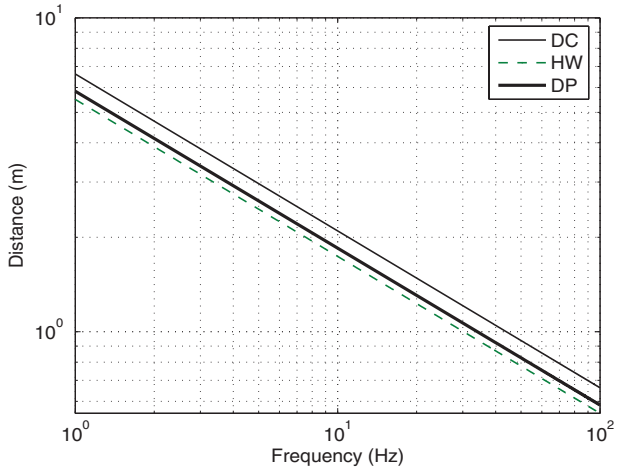

Figure 11 Near-field distances in the drilling pipes of Table 1 (unstressed). The linear relationship on the log-log plot is expected because of the proportionality between the distance $1/k_0$ and the reciprocal of the square root of frequency.

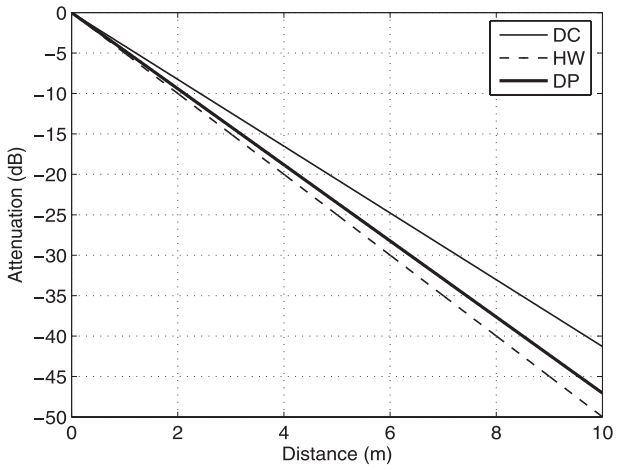

Figure 12 Attenuation of the standing resonant modes versus axial distance from the excitation point in the drill-string sections of Table 1 (unstressed). The curves are calculated for a signal of 10 Hz.

accurate for band-limited periodic functions with cut off spatial wavenumbers that are smaller than the cut off wavenumbers of the mesh. We use a spatial grid with interval $\Delta z = 1$ m, a time step of 2.5×10^{-4} s and maximum propagation time of 5 s. Let us consider the far-field in the pipe sections. We make use of the relation between shear force $\mathcal{F}$ and transverse particle velocity (time derivative of the deflection), given by equation (24). We set the analytic input signal to match the shear force of the direct solver with an injected source signal. The injected source signal $\mathcal{F}$ is implemented by spatial integration of a zero-phase signal with a smooth and band-limited amplitude spectrum between 10 and 50 Hz [Hanning window (Oppenheim and Schafer 1975)]. The time history of the injected source signal is shown in Fig. 13(a), where its maximum amplitude is 1 kN. The injected signal is shown together with the constitutive force response at the source location in the uniform DC section, calculated by Hilbert transforming the injected signal. The time history of the total shear force (total $\mathcal{F}$), sum of the injected signal and the pipe response, is shown in Fig. 13(b), which compares the analytical source signal (total $\mathcal{F}$) and the constitutive force signal measured at the source location obtained with the pseudospectral method.

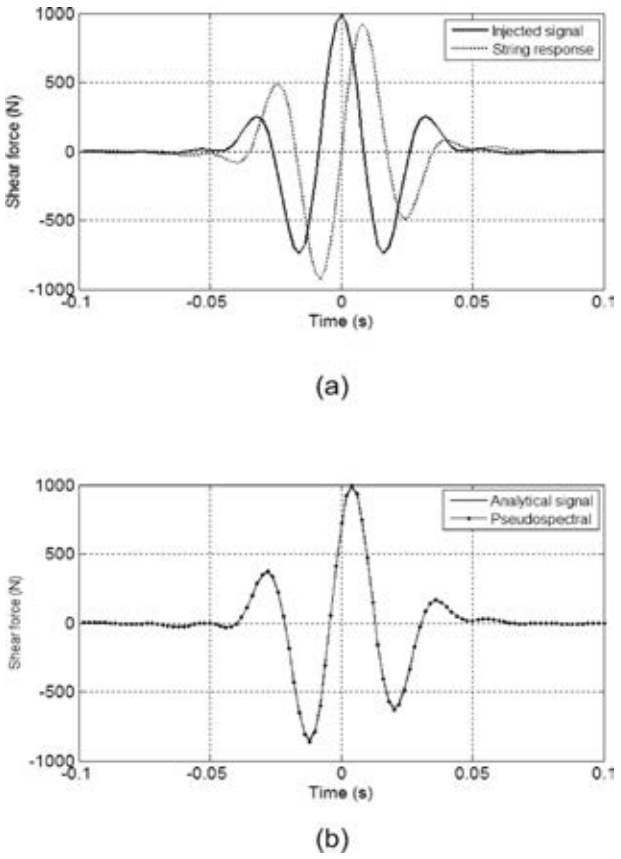

Figure 13 Input shearforce ($\mathcal{F}$) used to calculate the propagating waves in the DC section (a). The injected signal is represented by the black solid line. The dashed line represents the analytical constitutive response of the DC pipe, obtained by Hilbert transforming the injected signal. Total stress force in the DC section (b). The continuous line is the sum of the analytical input and the response signals of Fig. 13(a). The dotted line is the force measured at the source point in the DC section of the model used to calculate the full-wave (pseudospectral) solution.

The agreement is excellent. These signals are used later to test the present algorithm with the pseudospectral method, i.e., to normalize the input source $s(t)$ and for verification of the method in the calculation of the transmitted $\dot{w}_{\mathrm{T}}$ and reflected $\dot{w}_{\mathrm{R}}$ wavefields.

We now consider the DC/HWDP and HWDP/DP interfaces and compute the respective reflection and transmission coefficients. Table 2 shows the reflection and transmission coefficients determined with the unstressed drill string. Before computing the wavefields in the drill string shown in Fig. 5, we check the wave-mode coefficients R_w, T_w, R'_w and T'_w, verifying the wave propagation in a drill string composed by only two uniform tubes of different properties, as shown in Fig. 3.

Table 2 Reflection and transmission coefficients (unstressed case)

DC/HWDP interface			
Coefficient		Absolute value	Phase (degrees)
R_w	$-0.066 - \mathrm{i}\,0.290$	0.297	−103
R_s	$0.431 - \mathrm{i}\,0.431$	0.610	−45
T_w	1.963	1.963	0
T_s	$-0.598 - \mathrm{i}\,0.721$	0.937	−130
R'_w	$0.066 - \mathrm{i}\,0.290$	0.297	−77
R'_s	$-0.431 + \mathrm{i}\,0.431$	0.610	135
T'_w	0.464	0.464	0
T'_s	$0.171 + \mathrm{i}\,0.141$	0.222	40
HWDP/DP interface			
Coefficient		Absolute value	Phase (degrees)
R_w	$0.028 - \mathrm{i}\,0.069$	0.074	−68
R_s	$0.192 - \mathrm{i}\,0.192$	0.271	−45
T_w	1.497	1.497	0
T_s	$-0.277 - \mathrm{i}\,0.261$	0.381	−137
R'_w	$-0.028 - \mathrm{i}\,0.069$	0.074	−112
R'_s	$-0.192 + \mathrm{i}\,0.192$	0.271	135
T'_w	0.664	0.664	0
T'_s	$0.116 + \mathrm{i}\,0.123$	0.169	47

The source and the receiver are located at 250 m from the interface between T1 and T2, at opposite sides to compute $\dot{w}_{\mathrm{T}}$ and $\dot{w}_{\mathrm{R}}$. The propagation-matrix results are compared to those of the pseudospectral method. Before the comparison, the data are scaled to normalize the amplitude of the source, the total $\mathcal{F}$ shear force, to obtain a peak force of 1000 N. The comparison (true amplitude) is shown in Fig. 14, which includes transmitted waves, reflected waves and a test of the reciprocity principle, to further verify the algorithm. Reciprocity gives the same particle velocity in T2 and T1 when we use the same input force in T1 and T2 (Mace 1984).

Using the wave-mode reflection and transmission coefficients at the tubular interfaces, we calculate the wavefields corresponding to the string shown in Fig. 5. We compute the response given by equations (50) and (51). Figure 15 shows the signals $\dot{w}_{\mathrm{T}}$ and $\dot{w}_{\mathrm{R}}$ in a drill string without axial gravity loads and without boundary conditions at the bit obtained with the pseudospectral method (a) and propagation-matrix method (b), to test the far-field response of the structural system with multiple reflecting layers. The source is located at the bit and the receiver of the transmitted signal is located in the drill pipe, 500 m above the HWDP/DP interface, while the receiver recording the reflected signal is located at the bit

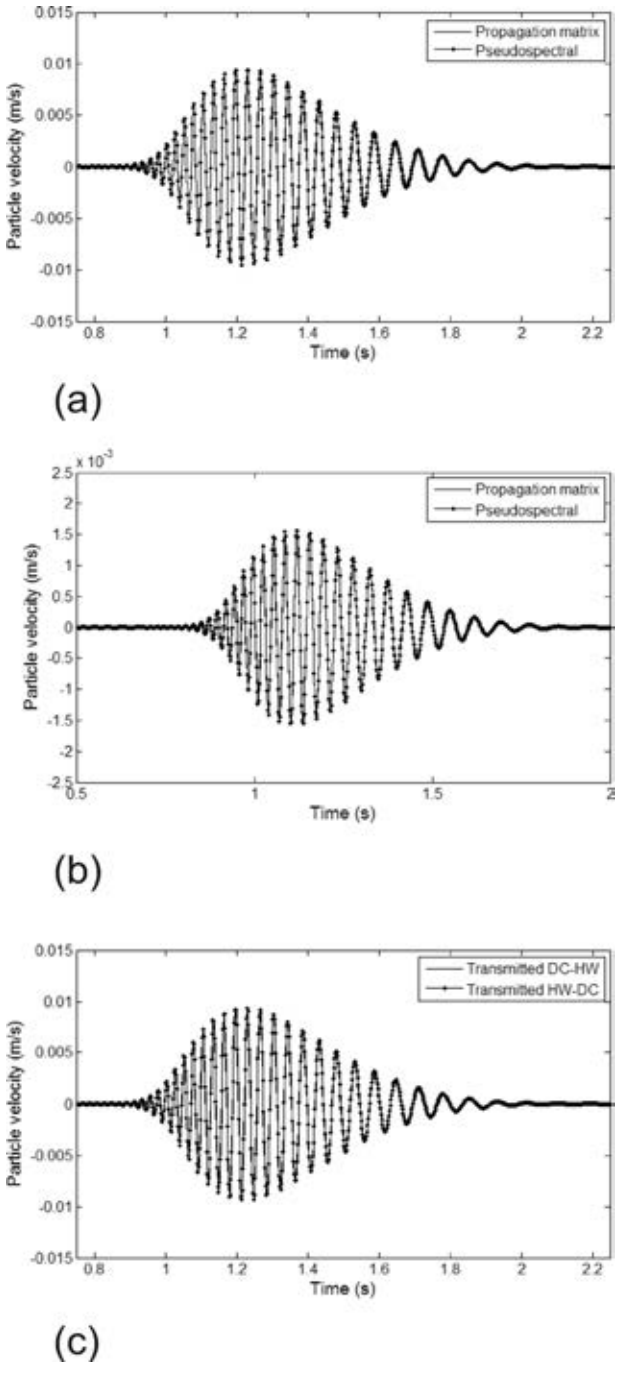

Figure 14 Comparison of wavefields obtained by the propagation-matrix and pseudospectral methods. Sources and receivers are located at 250 m distance from the interface between two semi-infinite pipe sections. a) Transmitted $\dot{w}_T(t)$ signal from DC to HWDP through the DC/HWDP interface (a). b) Reflected $\dot{w}_R(t)$ signal in the DC from the DC/HWDP interface (b). These signals satisfy reciprocity (c), where the matrix-propagated signals from DC to HWDP and vice versa, after normalizing the input forces, are compared.

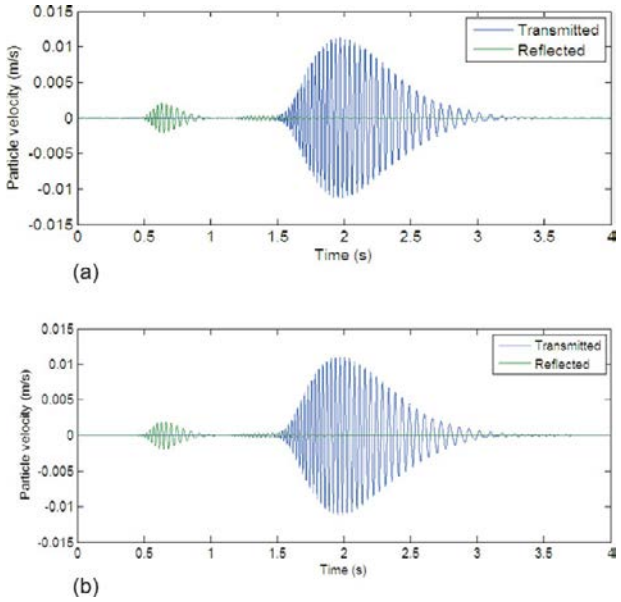

Figure 15 Transmitted $\dot{w}_T(t)$ and reflected $\dot{w}_R(t)$ waves from a source (shear force of Fig. 13a,b) applied in the drill collar section (DC) at the bit location. The results are obtained with a receiver in the drill pipe (DP) located 500 m above the heavy-weight (HWDP) pipe section in the drill string of Fig. 5, without a free-boundary end at the bit and without axial gravity loads. The result of the pseudospectral method (a) is compared to that of the propagation-matrix method (b). The agreement is excellent.

position. The upper side of the drill pipe is unbounded (DP of infinite length). The event at 0.65 s group delay is the two-way time reflection in the 145 m DC section and the event at about 2 s group delay is the transmitted signal through the 145 m DC, 145 m HWDP and 500 m DP. The signals are presented in true amplitude, after normalizing the source magnitude. The match is excellent.

Next, the signals are calculated assuming reflection conditions at the bit without pre-stress by axial gravity. In the following examples, we use a free boundary at the bit end. Other responses can easily be modelled by changing the boundary conditions at the string end. For example, assuming the fixed boundary condition end at the bit (equation (38)), we obtain $R_w = -\mathrm{i}$ as with the free end (equation (39)), which gives the same propagation matrix but with a modified source signal s due to the different impedances related to opposite near-field responses R_s at the source location. Figure 16 shows the time history of the transmitted and reflected waves in the drill string with the free boundary condition at the bit (modelled as a part of the DC), using the pseudospectral method (a) and the propagation-matrix method (b) numerical results. The free boundary is approximated in (a) by a very thin rod

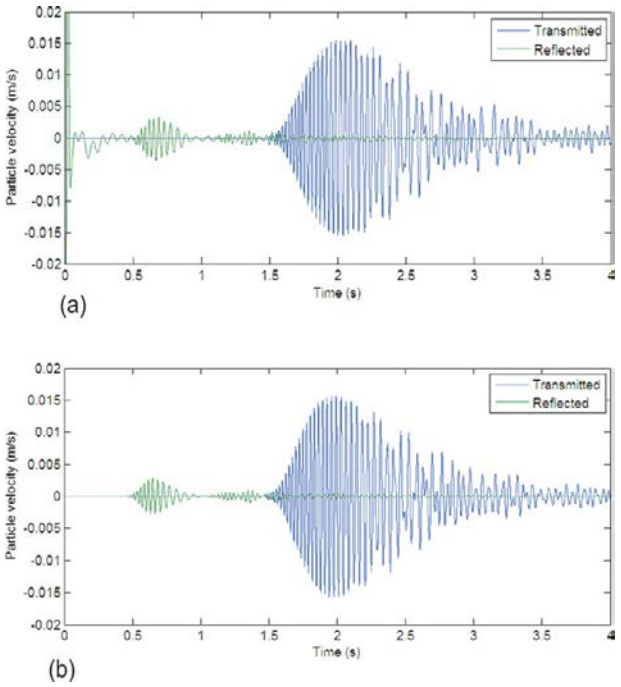

Figure 16 Transmitted $\dot{w}_T(t)$ and reflected $\dot{w}_R(t)$ waves from a source (shear force of Fig. 13a,b) applied to the DC section at the bit location in the drill string of Fig. 5. The bit is a free-boundary and the signals are calculated without axial gravity loads, with a receiver in the DP 500 m above the HWDP pipe section. Pseudospectral method (a) and propagation matrix method (b). At the origin in (a) we can see the source-signal reflection event and fluctuations due to the free-boundary approximation. The agreement is very good beyond 0.5 s.

(with inner and outer diameters 0.01 m and 0.011 m) below the bit. The initial spike ($t < 0.5$ s) for the reflection signal in (a) is the source signature measured at the source recording position, not modelled in the reflected analytic signal (b). The agreement is very good.

Finally, we calculate the propagation in strings with axial loads. We compute transient waves by integrating the delayed signals in the frequency domain. Let z_s and z_r be the source and receiver positions, respectively. The offset is defined as the relative distance, $z_r - z_s$, between the receiver and source. The propagation delay is obtained by integrating the reciprocal of the velocity (see equation (42)), where the lower and upper limits are z_s and z_r, respectively. In the presence of an axial pre-stress gradient, v is complex and we obtain a complex delay, where the real and imaginary parts correspond to pure delay and attenuation, respectively. An example of propagation in a uniform DP without and with uniform load is shown in Fig. 17. In (a) we can see the modification of the

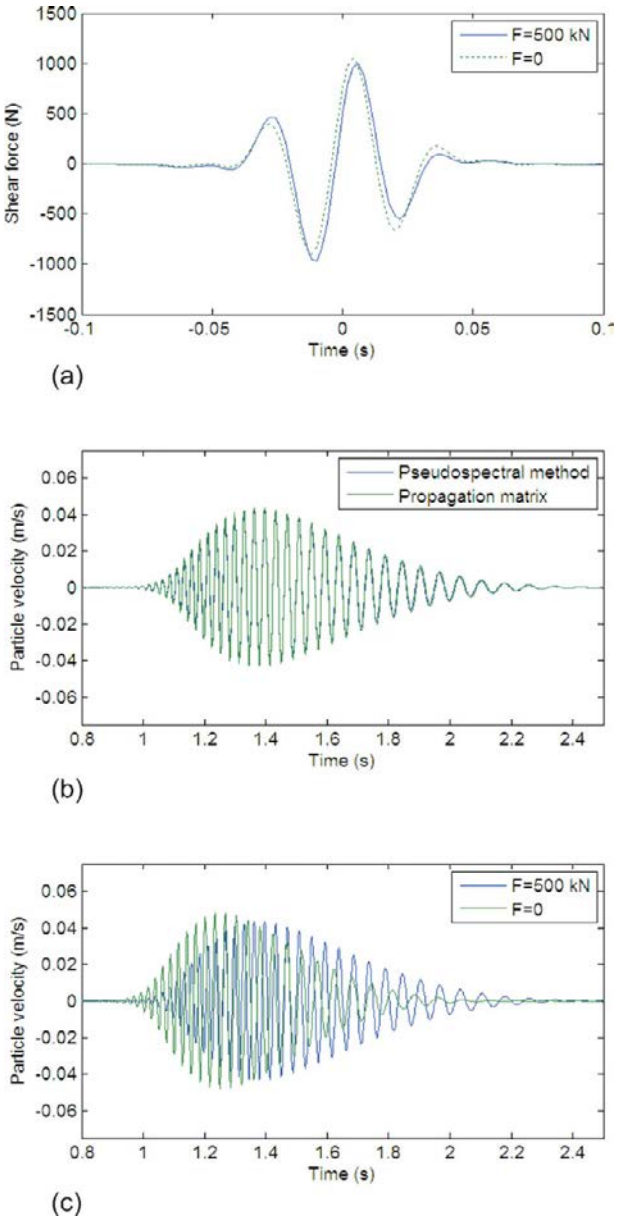

Figure 17 Shear source (total constitutive force) in a uniform DP section with and without uniform axial load (tension) (a). Pseudospectral and propagation-matrix transmitted wavefields $\dot{w}_T$ in an uniform drill pipe (DP) with constant tension conditions $F = 500$ kN (b). The agreement is very good. Propagation-matrix results with and without pre-loading (c). The group velocity in the pre-loaded case is lower and the group delay is higher (for a 500 kN axial force) compared to the unloaded case (in agreement with Fig. 6).

source signal (total constitutive shear force) due to the variation in the tension condition. Figure 17(b) shows the transmitted signals between the source and receiver at a distance of 500 m computed with the propagation-matrix and the pseudospectral methods with a uniform axial pre-load (tension) of

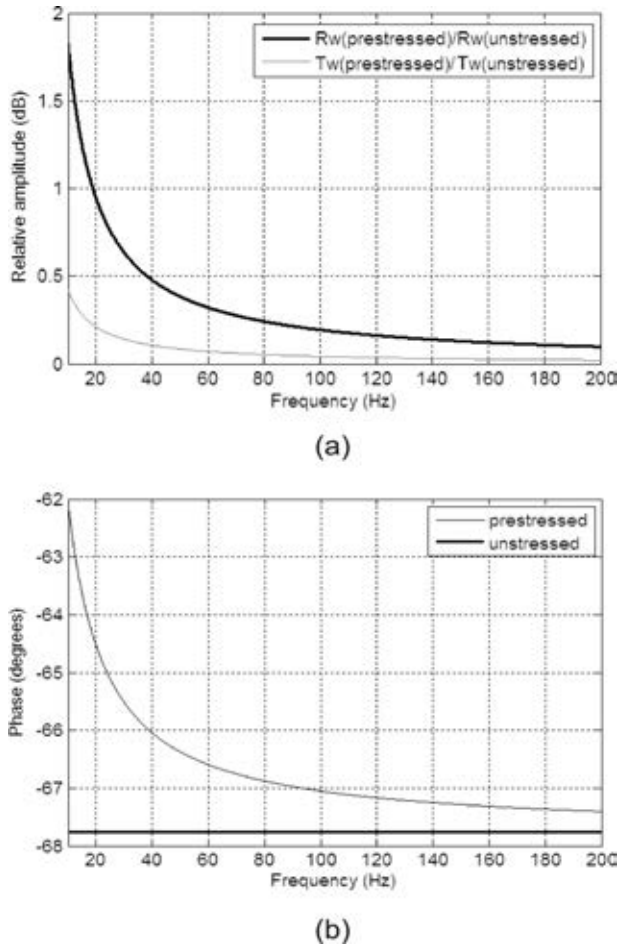

Figure 18 Absolute value of the ratio of the pre-stressed over unstressed reflection R_w and transmission T_w coefficients at the HWDP/DP interface (a). Phase of the reflection coefficient R_w at the HWDP/DP interface with and without pre-stress (b).

500 kN. Figure 17(c) compares the transmitted signals calculated with the propagation-matrix method with and without axial pre-loading. The effect of the axial tension (positive F) is to increase the phase velocity and to decrease the group velocity (see Fig. 6 b). Moreover, the reflection coefficients in strings with pre-load are frequency dependent.

Figure 18(a) displays the reflection and transmission, R_w and T_w, coefficients corresponding to the HWDP/DP interface with pre-stress. The curves are normalized with respect to the amplitude of the corresponding unstressed coefficients. The pre-stress is caused by the weight of the 145 m HWDP section (see Table 1). We observe that the variation in amplitude of the reflection coefficient is less than two dB at 10 Hz, while the variation in the amplitude of the transmission coefficient is much smaller. Figure 18(b) shows the phase of the pre-stressed

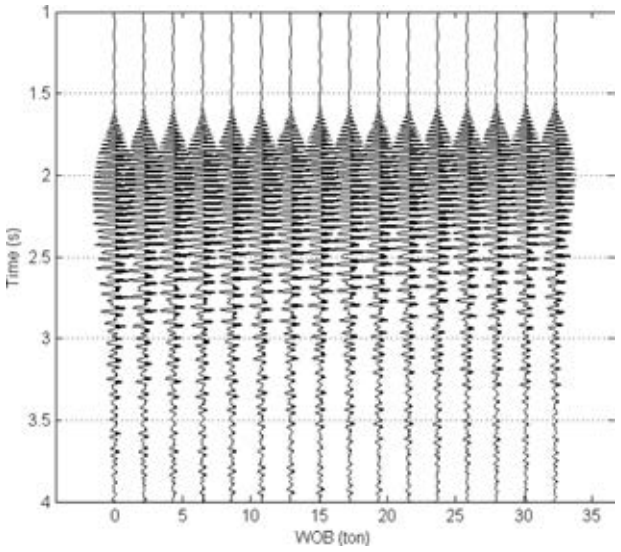

Figure 19 Results of the propagation-matrix method obtained with a receiver in the drill pipe (DP) 500 m above the heavy-weight (HWDP) pipe section of Fig. 5. The source is the shear force of Fig. 13 with the free boundary end at the bit. The waves represent transmitted signals $\dot{w}_T(t)$ in pre-stressed pipes with variable weight on bit (WOB). The waves are calculated with frequency-dependent (pre-stressed case) reflection coefficients including attenuation effects due to an axial load gradient (see Appendix). The group velocity decreases for lower pipe tensions, corresponding to higher WOB.

and unstressed coefficients. For both amplitude and phase, the effect is more important at lower frequencies. We include these effects in the propagation-matrix model. However, this analysis shows that a reasonable high-frequency approximation may be obtained using the unloaded reflection coefficients to model the propagation in the pre-stressed pipes.

We compute the transmission response given by equation (50) in the drill string open at the bottom of the DC. An equivalent result can be obtained for the reflection response. The source applied to the DC at the bit is the shear force of Fig. 13 in the bandwidth 10–50 Hz. The synthetic wavefields are calculated by using the unstressed drill-string model, including frequency dependent reflection coefficients and amplitude attenuation due to the gravity gradient. Figure 19 shows a gather of the pre-loaded signals. These traces are calculated with WOB ranging between 0–32 ton (320 kN). When the WOB = 0, the tension at the pipe includes the effect due to the weight of the 145 m DC section. Note that in this case all the string works in tension. Higher WOB corresponds to lower tension in the pipes. When WOB is greater than zero, part of the DC weight is unloaded and the lower DC section below the neutral point $z_{\rm NP} = WOB/(9.81\rho A_{\rm DC})$ works in compression.

However, due to the massive properties of the DC, there are no significant differences in the delays of the flexural waves in the DC section with variable pre-loading at the investigated frequencies. The variation in the propagation delay in the remaining part of the drill string is more important. In this figure, we can observe the variation in the signal waveform versus WOB. Even if the differences in the waveforms and delays of the signals are small for increments in WOB of a few tons, these changes are of the order of 50 ms in the total WOB interval. These delays are not negligible when the data are used for the analysis of events related to seismic signals. The observed group delays are in agreement with the calculated group velocity at the 30 Hz central frequency, ranging approximately between the averaged values $v_g \sim 385$ and $v_g \sim 395$ m/s. Similar calculations can be performed for the reflection response at the bit contact for SWD purposes.

DISCUSSION

In our analysis, no attenuation by viscoelastic effects – which would be expressed by a transverse resistive-type force – is included (however, the algorithm can easily be modified to include attenuation from energy dissipation). With this simplification, we neglect the coupling effects between the transverse drill-string vibrations and the acoustic borehole waves in the mud and surrounding formation (Malusa, Carcione and Poletto 2004). Also, the coupling between the flexural and axial vibration modes is neglected (Carcione and Poletto 2000). This effect is important in deviated wells (Drumheller 2002). Moreover, rotary and torsional effects on bending motions induced by rotation inertia of the pipes are neglected as well (Shyu 1989). These may result in unbalanced drilling conditions with bending resonances at critical rotary speeds (Mitchel and Allen 1985; Dunayewsky *et al.* 1993). In our model, the well is vertical, so that no bending forces are induced in the pipes due to the stretching of the pipe rotating in a borehole with curved trajectory (Vandiver *et al.* 1990; Bourgoyne *et al.* 1991). No contacts with the borehole wall are assumed, even if frequent contacts can be expected in correspondence of the string contact tools (stabilizers) (Shyu 1989; Bourgoyne *et al.* 1991; Poletto and Miranda 2004). Conversely, static tensile forces are included in the axial pre-stress equations. Mud buoyancy effects can be accounted for in the gravity tension as $F = \rho A g \mu h$, where $\mu \leq 1$ is a mud-buoyancy factor (Bourgoyne *et al.* 1991; Poletto and Miranda 2004). For simplicity, the mud buoyancy factor is $\mu = 1$ in our examples.

CONCLUSIONS

We present the results of a numerical approach for calculating the flexural reflection and transmission properties of drill strings in the thin-rod approximation. We have developed an analytical model and a propagation-matrix algorithm to simulate the drill-string flexural vibrations, to perform dispersion analysis of the radiated and resonant modes and to calculate the filtration of the reflections in vertical boreholes. The algorithm includes the axial gravity loads and the attenuation of far-field waves due to axial pre-stress gradients. Without loss of generality, we perform the analysis for typical seismic frequencies, such as those used for SWD purposes. This gives useful results to evaluate borehole seismic measurements in the presence of the drill string.

The dispersion equations are calculated for the different drill-string sections with and without axial pre-stress. The analysis shows that the reflection and transmission coefficients between different tubulars weakly depend on frequency only in the pre-stressed pipes. The near-field effects, related to the local resonant modes, can be neglected in the propagation model of a structural drill string with typical properties. However, once the propagating waves are calculated, the local resonant modes produced by the arrivals of the propagating waves at the pipe discontinuities can be derived.

We have used the far-field approximation to simulate the transmitted and reflected wavefields in a drill string of realistic geometry composed of a bottom-hole assembly and drill pipes, where we considered signals from sources acting in the seismic frequency range. The method is tested with unbounded and free boundary conditions at the bit end. The responses are compared with those of a full-wave direct solver for validation purposes. The analysis shows that the gravity pre-stress affects the wavefields obtained with different weight on bit (WOB) acting on the same pipe, working both in tension and compression. Increasing tension corresponds to an increase in the group delay of the flexural waves.

ACKNOWLEDGEMENTS

We thank Biancamaria Farina for useful comments.

REFERENCES

Barnes T.G. and Kirkwood B.R. 1972. Passbands for acoustic transmission in an idealized drill string. *Journal of the Acoustical Society of America* **52**, 1606–1608.

Bourgoyne A.T.J., Millheim K.K., Chenevert M.E. and Young F.S.J. 1991. *Applied Drilling Engineering*, SPE Textbook series, Vol. 2, Richardson, TX, USA.

Carcione J.M. 2007. *Wave fields in real media: Theory and Numerical Simulation of Wave Propagation in Anisotropic, Anelastic, Porous and Electromagnetic Media*. Second Edition. Elsevier Science, Amsterdam.

Carcione J.M. and Poletto F. 2000. Simulation of stress waves in attenuating drill strings, including piezoelectric sources and sensors. *Journal of the Acoustical Society of America* **108**, 53–64.

Chin W.C. 1988. Why drill strings fail at the neutral point. *Petroleum engineering international* **5**, 62–67.

Chin W.C. 1994. *Wave Propagation in Petroleum Engineering*. Gulf Publishing Company.

Connaire A., O'Sullivan E., Carr T. and Witton M. 2008. Advancements in methods for quantifying energy dissipation in unbounded flexible pipe. Offshore Technology Conference, Paper 19705-MS.

Drumheller D.S. 1993. Coupled extensional and bending motion in elastic waveguides. *Wave Motion* **17**, 319–327.

Drumheller D.S. 2002. Wave impedances of drill strings and other periodic media. *Journal of the Acoustical Society of America* **112**, 2527–2539.

Dunayewsky V.A., Abbassian F. and Judzis A. 1993. Dynamic stability of drillstrings under fluctuating weight on bit. *SPE Drilling & Completion*, 84–92.

Graff K.F. 1975. *Wave Motion in Elastic Solids*. Dover Publications, Inc, New York.

Guo Y.P. 1995. Flexural wave transmission through angled structural joints. *Journal of the Acoustical Society of America* **97**, 289–297.

Kolsky H. 1953. *Stress waves in solids*. Oxford University Press.

Lebedev A. and Beresnev I. 2005. Radiation from flexural vibrations of the baseplate and their effect on the accuracy of traveltime measurements. *Geophysical Prospecting* **53**, 543–555.

Lee S.-K., Mace B.R. and Brennan M.J. 2007. Wave propagation, reflection and transmission in curved beams,. *Journal of Sound and Vibration* **306**, 636–656.

Lindsay R.B. 1934. Filtration of elastic waves in solid rods. *Journal of the Acoustical Society of America* **5**, 196–201.

Love A.E.H. 1952. *A Treatise on the Mathematical Theory of Elasticity*. Cambridge University Press.

Mace B.R. 1984. Wave reflection and transmission in beams. *Journal of Sound and Vibration* **97**, 237–246.

Mace B.R. 1992. Reciprocity, conservation of energy and some properties of reflection and transmission coefficients. *Journal of Sound and Vibration* **155**, 375–381.

MacPherson J.D., Mason J.S. and Kingman J.E.E. 1993. Surface measurement and analysis of drill string vibrations while drilling. SPE/IADC Paper No. 25777.

Malusa M., Carcione J.M. and Poletto F. 2005. Coupled axial waves in drill strings, Expanded Abstract, 67th EAGE Conference and Exhibition.

Mitchell R.F. and Allen M.B. 1985. Lateral vibration: The key to BHA failure analysis. *World Oil*, March Issue. 400, 101–104.

Muggleton J.M., Waters T.P., Mace B.R. and Zhang T. 2007. Approaches to estimating the reflection and transmission coefficients of discontinuities in waveguides. *Journal of Sound and Vibration* **307**, 280–294.

Oppenheim A.V. and Schafer R.W. 1975. *Digital Signal Processing*. Prentice-Hall, Englewood Cliffs, New York.

Poletto F. and Miranda F. 2004. *Seismic While Drilling. Fundamentals of Drill Bit Seismic for Exploration*. Elsevier Science, Amsterdam.

Sablik M.J. 1982. Coupling loss factors at a beam L-joint revisited. *Journal of the Acoustical Society of America* **72**, 1285–1288.

Shyu R.J. 1989. Bending vibration of rotating drill string, Ph.D. thesis, MIT Thesis.

Sinha B.K. and Asvadurov S. 2004. Dispersion and radial depth of investigation of borehole modes. *Geophysical Prospecting* **52**, 271–286.

Vandiver J.K., Nicholson J.W. and Shyu R.J. 1990. Case studies of the bending vibration and whirling motion of drill collars. SPE Drilling Engineering, SPE Paper no. 18652, 282–290.

White J.E. 1965. *Seismic Waves: Radiation, Transmission, and Attenuation*. McGraw-Hill Book Company, New York.

Wolf S.F., Zacksenhouse M. and Arian A. 1985. Field measurements of downhole drillstring vibrations, SPE Paper No. 14330.

Zannoni S.A., Cheatham C.A., Chen C.-K.D. and Golla C.A. 1993. Development and field testing of new downhole MWD drillstring dynamics sensor. SPE Paper No. 26341.

APPENDIX: COMPLEX WAVENUMBERS

Uniform pipe with a pre-stress gradient

The solutions of dispersion equation (9) with a pre-stress gradient different from zero are:

$$k_{1,2,3,4} = \pm\frac{1}{2}\sqrt{-\frac{4b}{3}+\Theta} \pm \frac{1}{2}\sqrt{-\frac{8b}{3}-\Theta+\frac{2ic}{\sqrt{-4b/3+\Theta}}}, \tag{A1}$$

where

$$\Theta = \frac{\chi}{3(2^{1/3})} + \frac{4(2^{1/3})(b^2-3a^2\omega^2)}{3\chi}, \tag{A2}$$

with

$$\chi = \sqrt[3]{16b^3-27c^2+144ba^2\omega^2+\sqrt{-4(4b^2-12a^2\omega^2)^3+(16b^3-27c^2+144ba^2\omega^2)^2}}. \tag{A3}$$

Solution at the neutral point

The solutions of the dispersion equation with a pre-stress gradient ($c \neq 0$) at the neutral point ($b = 0$) are

$$k_{1,2,3,4} = \pm\frac{\sqrt{\Theta}}{2} \pm \frac{1}{2}\sqrt{-\Theta+\frac{2ic}{\sqrt{\Theta}}}, \tag{A4}$$

where

$$\Theta = \frac{\sqrt[3]{-9c^2+\sqrt{3(27c^4+256a^6\omega^6)}}}{2^{1/3}3^{2/3}} - \frac{4(2/3)^{1/3}a^2\omega^2}{\sqrt[3]{-9c^2+\sqrt{3(27c^4+256a^6\omega^6)}}}. \tag{A5}$$